Experimental Realization of Nonunitary Multiqubit Operations

M. W. van Mourik,[1] E. Zapusek,[2] P. Hrmo,[1] L. Gerster,[1] R. Blatt,[1] T. Monz,[1,3] P. Schindler,[1] and F. Reiter[2]
[1]Institut für Experimentalphysik, Universität Innsbruck, Technikerstraße 25/4, 6020 Innsbruck, Austria
[2]Institute for Quantum Electronics, ETH Zürich, Otto-Stern-Weg 1, 8093 Zürich, Switzerland
[3]AQT, Technikerstraße 17, 6020 Innsbruck, Austria

(Received 7 April 2023; accepted 13 November 2023; published 23 January 2024)

We demonstrate a novel experimental tool set that enables irreversible multiqubit operations on a quantum platform. To exemplify our approach, we realize two elementary nonunitary operations: the OR and NOR gates. The electronic states of two trapped $^{40}Ca^{+}$ ions encode the logical information, and a cotrapped $^{88}Sr^{+}$ ion provides the irreversibility of the gate by a dissipation channel through sideband cooling. We measure 87% and 81% success rates for the OR and NOR gates, respectively. The presented methods are a stepping stone toward other nonunitary operations such as in quantum error correction and quantum machine learning.

DOI: 10.1103/PhysRevLett.132.040602

Introduction.—Classical computing is an immensely successful information processing paradigm. The success of computing can largely be explained by the rapid increase in computational power enabled by the miniaturization of the underlying circuits built from classical, irreversible gate operations [cf. Fig. 1(a)]. Today, the exponential growth of gate count on classical processors is reaching fundamental physical limits [1]. In the continued pursuit of increasing computational power, a multitude of alternate technologies is being explored [2–13].

As an approach orthogonal to classical information processing, quantum computing has recently received considerable attention. Here, substantial advancements have been made, allowing for first demonstrations of essential ingredients such as quantum error correction [14–19]. This can be attributed to novel and advanced proposals and the continued improvement of established techniques [20–24]. Such advancements bring quantum computation closer to the ideal of an entirely unitary evolution toward the output state. In certain algorithms, however, *nonunitary* operations are required in combination with unitary quantum gates. Among these are algorithms for quantum machine learning, quantum optimization, and simulation, which are regarded as some of the most promising near-term applications for quantum information processing [18,25–38]. Specifically, nonunitary operations are needed for the generation of low-temperature thermal states [27–30], as a projective filter [31], for the simulation of open systems [32–37], or in quantum neural networks [18,38]. Furthermore, nonunitary operations can reduce the entropy of a system, allowing for the robust preparation of many-body states and even fault-tolerant quantum error correction [39–41]. It has been suggested to implement nonunitary components through auxiliary qubits, randomized circuits, or mixed input states [27,30–36].

Dissipation is inherently nonunitary, making it a natural choice for the creation of irreversible operations. The field of dissipation engineering, or reservoir engineering, uses the interaction of a quantum system with environmental degrees of freedom to achieve quantum information processing tasks [39,42–54]. Applications include state preparation by optical pumping, squeezing [43,44], entanglement generation [45–52], quantum simulation [53], and quantum error correction [39]. Dissipation toward the environment lifts the requirement for classical measurement and feedback, and it holds scaling and robustness advantages over unitary approaches [46–48]. It has been formally shown that dissipation can be used to perform universal quantum computation [55]. Still, so far, dissipation engineering has mostly been focused on quantum state preparation and subspace stabilization. We expand the possible set of applications taking a step toward a paradigm of general nonunitary quantum operations, by

(a)

OR		NOR	
In	Out	In	Out
$\|00\rangle$	$\|00\rangle$	$\|00\rangle$	$\|10\rangle$
$\|01\rangle$	$\|11\rangle$	$\|01\rangle$	$\|01\rangle$
$\|10\rangle$	$\|10\rangle$	$\|10\rangle$	$\|00\rangle$
$\|11\rangle$	$\|11\rangle$	$\|11\rangle$	$\|01\rangle$

(b)

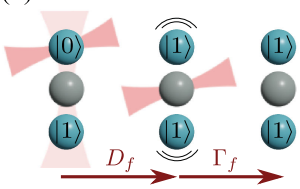

FIG. 1. (a) Truth tables of the classical OR and NOR gates, with two-qubit output. The logical output is mapped on the left qubit. (b) Schematic representation of the OR gate acting on a pair of ions in the $|01\rangle$ state: An engineered resonance process D_f is a combination of a global and single-ion laser pulse, which together allow transfer to the desired state $|11\rangle$, plus an increase in motional mode occupation. This action is made irreversible by dissipation Γ_f of this additional motion, by cooling a spectator ion species.

demonstrating the realization of irreversible classical gates [cf. Fig. 1(a)] by means of engineered dissipation.

Here, we present a physical realization of nonunitary operations in a trapped-ion system by use of dissipation engineering. By utilizing techniques from dissipation engineering, one can create nonunitary quantum gates that operate deterministically and without the need for ancilla qubits [56]. To this end, from quantum-mechanical interactions, we engineer the desired projective dynamics effecting classical gate operations. We implement a classical OR and NOR gate, whose truth tables are shown in Fig. 1(a), where the output of the gate action is mapped onto the left qubit. We employ selective coherent couplings to conditionally excite electronic states, utilizing the ions' shared motional modes, schematically outlined in Fig. 1(b). Sympathetic cooling serves as the nonunitary component and completes the gate action. Experimentally, the desired dynamics can be implemented in a mixed-species trapped-ion system with single-qubit addressing capabilities [57]. Our operations differ from dissipative state preparation schemes [45–52], which generate a predetermined output state regardless of the input state. The demonstration of classical gates is the first multiqubit nonunitary gate operation. Through our work, we show that carefully engineered nonunitary quantum dynamics have the potential to enrich the quantum engineer's toolbox, by performing a broad class of operations that includes any Markovian evolution of two qubits [58]. The nonunitary gates we demonstrate open up applications in a wide range of quantum information algorithms. In particular, they represent a significant advancement toward autonomous error correction, as they utilize the same couplings as described in Ref. [39].

Principle of operation.—Two cotrapped $^{40}Ca^{+}$ ions serve as information carriers, with the logical states $|0\rangle$ and $|1\rangle$ encoded in the $4S_{1/2}(m=-1/2)$ and $(m=+1/2)$ Zeeman sublevels [see Fig. 2(a)]. The ions are trapped in a harmonic potential and share motional modes. We use the notation $|i\rangle_1 \otimes |j\rangle_2 \otimes |n\rangle_m = |ij\rangle|n\rangle_m$ for electronic states i and j of ions 1 and 2 and mode occupation n of the in-phase motional mode m. For brevity, the mode occupation n is often omitted in our notation when $n=0$, i.e., $|ij\rangle = |ij\rangle|0\rangle_m$. As seen in the truth table in Fig. 1(a), the OR gate corresponds to the mapping of $|01\rangle$ to $|11\rangle$, which is analogous to the condition that the first qubit is flipped from $|0\rangle$ to $|1\rangle$ if and only if the second qubit is the state $|1\rangle$. The desired conditional operation is augmented by making use of the motional mode to encode information about the parity of the system. Access to this mode is enabled through the auxiliary state $|f\rangle$, for which we use the metastable $3D_{5/2}(m=+1/2)$ level. The $4S_{1/2} \leftrightarrow 3D_{5/2}$ transition to this auxiliary state is coupled with coherent 729 nm light.

The population transfer mechanism is summarized below (details in [62]). A drive with Rabi frequency Ω_f and detuning Δ is applied to the first ion's $|0\rangle \leftrightarrow |f\rangle$ transition. We refer to this drive as the probe. Without any further couplings, the probe would excite the two states $|00\rangle$ and $|01\rangle$ and leave the states $|10\rangle$ and $|11\rangle$ unchanged. A second drive, which we refer to as the sideband drive, is applied to both ions on the $|f\rangle \leftrightarrow |1\rangle$ transition, though red-detuned by the frequency of the motional mode. This drive, therefore, couples the states $|f\rangle|n\rangle_m \leftrightarrow |1\rangle|n+1\rangle_m$.

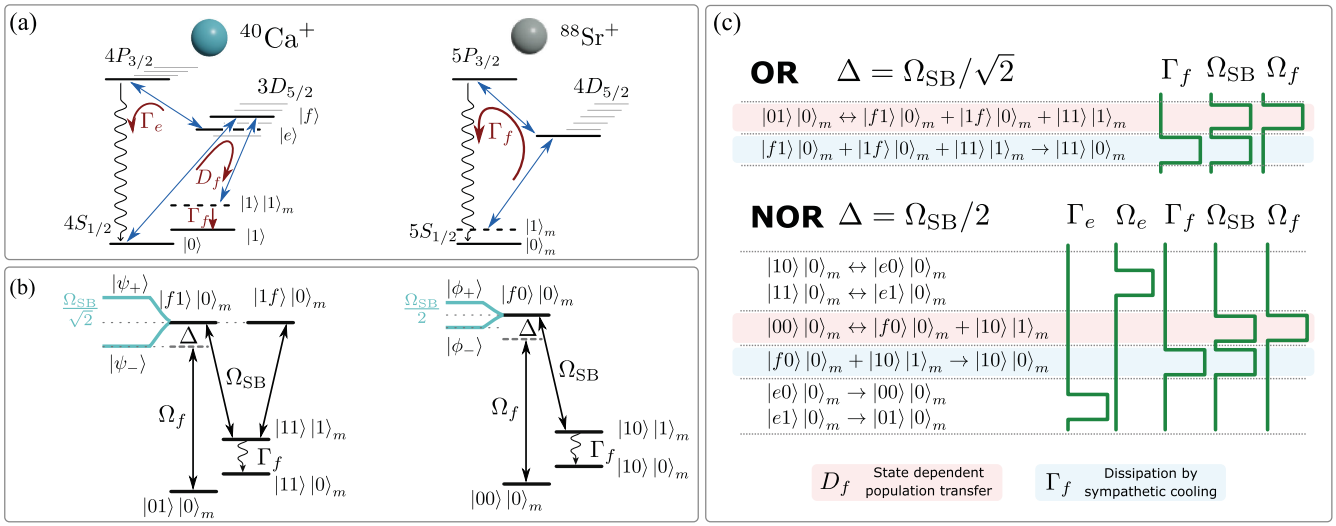

FIG. 2. Overview of the gate mechanism. (a) Relevant states in the data ions $^{40}Ca^{+}$ and cooling ion $^{88}Sr^{+}$. Logical bits $|0\rangle$ and $|1\rangle$ are stored in calcium's $4S_{1/2}$ ground states. Auxiliary levels in the $3D_{5/2}$ manifold are used for engineered resonance transfer D_f. Dissipation Γ_e and Γ_f occurs through spontaneous decay. (b) Dressed state generation, with a strong sideband drive Ω_{SB}. The desired conditional excitation for the OR and NOR gates are enabled by unequal detuning from the transition between the initial states $|01\rangle|0\rangle_m$ and $|00\rangle|0\rangle_m$ and the dressed states $|\psi_\pm\rangle$ and $|\phi_\pm\rangle$, by $\pm\Omega_{SB}/\sqrt{2}$ and $\pm\Omega_{SB}/2$. (c) Pulse sequence of OR and NOR gates. Ω_f and Ω_e act on the first ion, coupling $|0\rangle$ with $|f\rangle$ and $|1\rangle$ with $|e\rangle$. Ω_{SB} acts on both ions, coupling the red sideband of $|1\rangle$ and $|f\rangle$.

In particular, the transition between $|f\rangle|0\rangle_m \leftrightarrow |1\rangle|1\rangle_m$ occurs with Rabi frequency Ω_{SB}. Under the condition that $\Omega_{\mathrm{SB}} \gg \Omega_f$, the states excited from $|01\rangle|0\rangle_m$ form dressed states $|\psi_\pm\rangle = (|f1\rangle|0\rangle_m + |1f\rangle|0\rangle_m \pm \sqrt{2}|11\rangle|1\rangle_m)/2$. These dressed states have a frequency shift of $\pm\Omega_{\mathrm{SB}}/\sqrt{2}$, with respect to the bare $|f1\rangle|0\rangle_m$ state, as shown in Fig. 2(b), left. In contrast, the initial state $|00\rangle|0\rangle_m$ is excited to the dressed states $|\phi_\pm\rangle = (|f0\rangle|0\rangle_m \pm |10\rangle|1\rangle_m)/\sqrt{2}$ [Fig. 2(b), right], which reside at frequencies $\pm\Omega_{\mathrm{SB}}/2$. The three-level dressed states $|\psi_\pm\rangle$ have increased frequency shifts compared to the two-level dressed states $|\phi_\pm\rangle$ because of constructive interference of the couplings $\{|1f\rangle|0\rangle_m, |f1\rangle|0\rangle_m\} \leftrightarrow |11\rangle|1\rangle_m$. Choosing a probe pulse detuning $\Delta = \Omega_{\mathrm{SB}}/\sqrt{2}$, therefore, enables excitation from $|01\rangle$, while excitation from $|00\rangle$ is out of resonance and, thus, suppressed. This population transfer through engineered resonance is denoted by D_f in Fig. 2(a).

The conditional excitation is made nonunitary by a decay process enabled by sideband cooling a cotrapped $^{88}Sr^+$ ion, indicated by Γ_f in Fig. 2(a). In the OR gate, population that cycles through $|11\rangle|1\rangle_m$ is dissipatively transferred to $|11\rangle|0\rangle_m$ at a rate Γ_f. Since $|11\rangle|0\rangle_m$ does not couple with either the sideband drive or the probe, population remains in this state, thus completing the transfer $|01\rangle \rightarrow |11\rangle$. In order to avoid interfering with the excitation during the probe process, the dissipation is realized in a subsequent step [47,51].

We demonstrate the universal NOR gate, whose truth table is shown in Fig. 1(a). This gate can be constructed by concatenating a unitary NOT gate with the OR gate. However, we present a fully dissipative implementation where the mapping $|00\rangle \rightarrow |10\rangle$ follows the same procedure as the OR gate. In contrast to the OR gate, for the NOR gate we use the detuning $\Delta = \Omega_{\mathrm{SB}}/2$ to excite the initial state $|00\rangle$. In addition, the transfers $|11\rangle \rightarrow |01\rangle$ and $|10\rangle \rightarrow |00\rangle$ are required for the gate action which can be implemented by a single-qubit dissipative process. Both mappings are achieved by optically pumping the first ion from $|1\rangle$ to $|0\rangle$ over another auxiliary level, $3D_{5/2}(m = -3/2) \equiv |e\rangle$, and subsequently to $4P_{3/2}(m = -3/2)$, from where spontaneous decay returns population to the $|0\rangle$ state.

Experimental overview.—The experiments have been carried out with a segmented surface trap in a cryogenic environment [57]. Ions are stored in the Ca-Sr-Ca configuration [63,64]. Ions are initialized in $|00\rangle$ using optical pumping and are sideband cooled to a mean mode occupation of 0.14 phonons in the axial in-phase (ip) mode. We prepare the remaining possible initial states $|01\rangle$, $|10\rangle$, and $|11\rangle$, using a combination of single-ion and collective π pulses on the $|0\rangle \leftrightarrow |f\rangle$ and $|f\rangle \leftrightarrow |1\rangle$ transitions.

The sequences of pulses for the OR and NOR operations are schematically shown in Fig. 2(c), referring to the states shown in Fig. 2(a), with Ω_f and Ω_e acting only on the first ion, coupling $|0\rangle$ with $|f\rangle$ and $|1\rangle$ with $|e\rangle$, respectively. Ω_{SB} acts on both ions and couples the red sideband of $|1\rangle$ and $|f\rangle$.

The splitting of the dressed states $|\phi_\pm\rangle$ and $|\psi_\pm\rangle$ is produced with a sideband drive with Rabi frequency $\Omega_{\mathrm{SB}}/(2\pi) \approx 8$ kHz, as shown in Fig. 2(b). The probe beam, simultaneously applied to only the first ion, has an on-resonance Rabi frequency of $\Omega_f/(2\pi) \approx 1.15$ kHz. For the OR gate, these pulses are applied for a duration of $2\pi/\Omega_f = 900$ μs, at a detuning $\Delta = \Omega_{\mathrm{SB}}/\sqrt{2}$, which excites $|01\rangle$ to the dressed state $|\psi_+\rangle$. The NOR gate has a duration of $\sqrt{2}\pi/\Omega_f \approx 600$ μs and a detuning $\Delta = \Omega_{\mathrm{SB}}/2$, exciting $|00\rangle$ to $|\phi_+\rangle$.

Following this state-dependent population transfer, in the OR gate, the state $|11\rangle|1\rangle_m$ is dissipatively transferred to $|11\rangle|0\rangle_m$ by cooling the Sr ion. Similarly, in the NOR gate, $|10\rangle|1\rangle_m$ is transferred to $|10\rangle|0\rangle_m$. The sideband coupling Ω_{SB} is maintained during the cooling step, which fully depletes the populated dressed state.

The additional channel of dissipation required by the NOR operation, $|1\rangle \rightarrow |0\rangle$ for only the first ion, is performed in multiple steps, since it would otherwise conflict with the simultaneously required $|00\rangle \rightarrow |10\rangle$ operation. Preceding the engineered dissipation, population in the first ion's $|1\rangle$ state is stored in $|e\rangle$. After the engineered dissipation, light at 854 nm transfers population in $|e\rangle$ to the $4P_{3/2}$ level. The polarization of the 854 nm light was adjusted to minimize decay to the $4S_{1/2}(m = +1/2) = |1\rangle$ state, by predominantly pumping to the $4P_{3/2}(m = -3/2)$ state.

At the end of the sequence, the population is read out with state-dependent fluorescence detection using an EMCCD camera, which distinguishes excitation of the S and D manifolds. As the logical information is carried in the two S levels [cf. Fig. 2(a)], the population in $|1\rangle$ needs to be transferred to $|e\rangle$ before the measurement. This state readout does not differentiate between $|1\rangle$ and $|f\rangle$. We use the notation P_{ij} to indicate the population in state $|ij\rangle$. We can separately measure the occupation of the motional mode by applying a pulse on resonance with either the red or blue sideband of one of the strontium ion's $5S_{1/2} \leftrightarrow 4D_{5/2}$ transitions and reading out its state [65]. The difference of the excitation probability of the red and blue sideband excitations is used to infer the population in the motional ground state.

Results.—We first demonstrate the central building block of resonance engineering, the state-dependent population transfer, by showing its time evolution, using a detuning of $\Delta = \Omega_{\mathrm{SB}}/2$. The change in population is shown for all four initial states. The intended behavior, Rabi cycling from $|00\rangle$ and no transfer from the other initial states, is apparent in Fig. 3(a). The solid lines denote simulated data. The simulations numerically solve the system's master equation [62] and use experimentally determined

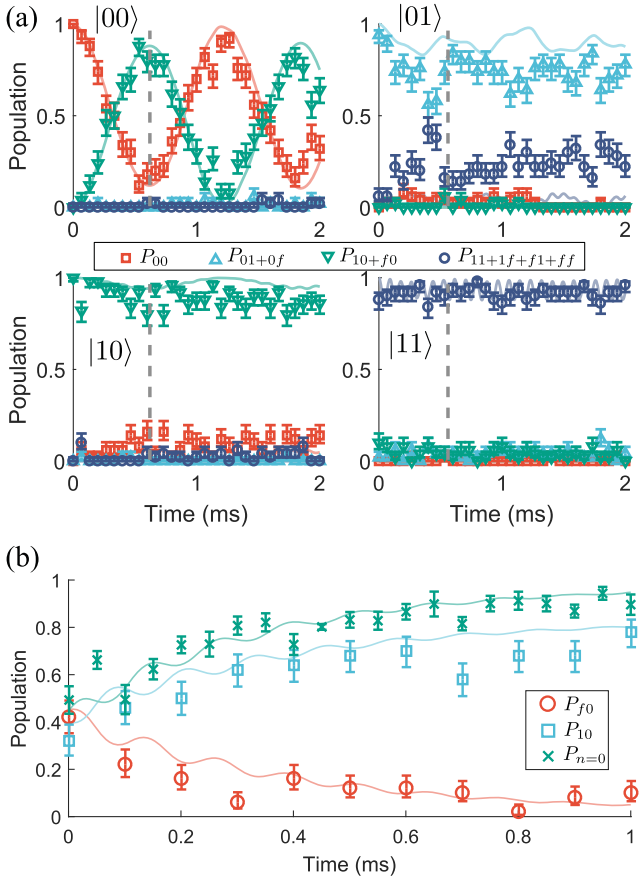

FIG. 3. (a) Experimental demonstration of state-dependent population transfer with $\Delta = \Omega_{SB}/2$, shown for each possible initial state. The lines indicate simulated results. (b) Demonstration of dissipation, after a maximal probe transfer from $|00\rangle$ [at a time marked by the gray dashed line in (a)]. We show the evolution of P_{f0} and P_{10} and the ground-state phonon occupation. The lines show simulated results.

parameters described above, including the initial phonon number ($\bar{n} = 0.14$) and heating rate [$\dot{\bar{n}} = 106(20)$ s^{-1}]. The gray dashed line marks the duration of the pulse with the maximum state transfer, 600 μs, where 82% of population has depleted from $|00\rangle$ (top left panel). The deviation from a full population transfer is attributed to the nonzero initial phonon number and heating rate, corroborated by the simulated results. With the ions prepared in the $|01\rangle$ state, only 16% of the population is depleted (top right panel).

After this population transfer, the state $|\phi_+\rangle = (|10\rangle|1\rangle_m + |f0\rangle|0\rangle_m)/\sqrt{2}$ should be dissipatively transferred to $|10\rangle|0\rangle_m$. We demonstrate this process by showing the evolution of the populations P_{f0} and P_{10} and the phonon ground-state occupation over time in Fig. 3(b). The electronic states are differentiated by running the measurement twice: once with the transfer of $|1\rangle$ to $|e\rangle$ and once without. The latter measurement does not discriminate between $|0\rangle$ and $|1\rangle$. The population P_{10} is inferred from

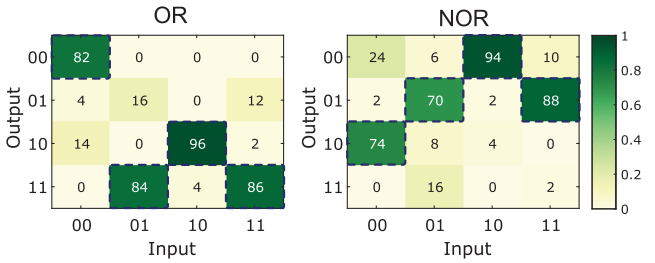

FIG. 4. Measured population truth tables of the OR and NOR gates, with the intended output states marked with dashed lines. Values are in percent and are determined from 50 experimental shots for each input setting. The OR and NOR gates have an average population fidelity of 87(5)% and 81(5)%, respectively.

the difference between the first and second measurements. We additionally measure the phonon occupation. The lines are simulated results, using the same sideband coupling strength Ω_{SB} as in Fig. 3(a). A dissipation rate of $\Gamma_f = 4.5(6)$ kHz is determined by a least-squares fit between the simulated and measured results. After 1 ms of applying the dissipation pulse, approximately 80% of the population is in $|10\rangle|0\rangle_m$.

Having demonstrated and characterized the engineered resonance and dissipation processes, we apply these steps within the full pulse sequences shown in Fig. 2(b) to perform the OR and NOR gates. Figure 4 shows the measured population outcome for each of the four possible initial states for the OR and NOR gates. Populations are determined from 50 experimental repetitions for each input state. Both truth tables exhibit the intended gate behavior: For all input states, the majority of the population is transferred to the desired state, marked in the figure with dashed boxes. The initial states $|01\rangle$ and $|00\rangle$ are transferred following the engineered resonance scheme for the OR and NOR gates, respectively, with success rates of 84(5)% and 74(6)%. The values in parentheses represent the statistical uncertainty from averaging over the 50 experimental repetitions. As confirmed by simulations and analytics [66], a dominant source of error is attributed to a nonzero initial phonon number and the heating rate. Since the coupling strength to a motional sideband is dependent on the phonon number, the resonance condition of the engineered population transfer is not met for $n \geq 1$. Another source of error is off-resonant excitation of the undesired population transfer as a result of spectral overlap with the resonance conditions of the desired population transfers, leading to 17% error in the OR gate and 5% in the NOR gate.

Conclusion and outlook.—We have implemented nonunitary multiqubit operations in a trapped-ion system by use of engineered dissipation. The schemes for the OR and NOR gate performed the operations with fidelities of 87(5)% and 81(5)%, respectively, where fidelity is the average of success rates over all possible initial states. This constitutes the first realization of dissipative quantum gate operations.

Further classes of operations can be realized according to these principles. In Supplemental Material [58], we detail how our experimental capabilities can emulate any Markovian two-qubit evolution.

The leading source of error stems from heating and, thus, imperfect cooling of the mode over which the intended dissipation process occurs. This heating process is the result of electronic noise on the trap surface and by phonon transfer from other uncooled motional modes caused by mode coupling, both of which are known challenges of microfabricated ion traps [67,68], and is further exacerbated by complications involved in mixed-species operation [64]. Such issues are technical and do not pose fundamental limitations: Future experiments could implement improved trap design and manufacturing to reduce heating due to technical noise and improved cooling techniques such as polarization gradient cooling [69] and electromagnetically-induced-transparency cooling [70]. Much like recent dissipative high-fidelity schemes for entangled state preparation [49–52] improved upon the fidelities of their first-generation counterparts, we would expect future implementations to improve the fidelity.

Errors caused by the undesired population transfer mechanism being off-resonantly excited (17% in the OR gate and 5% in the NOR gate) are also not a fundamental limitation: A higher pump-beam coupling Ω_{SB} splits the resonance conditions of the desired and undesired population transfers further, thus decreasing off-resonant excitation. For example, a doubling of Ω_{SB}, feasible with modern hardware improvements such as higher-power laser systems, would reduce the off-resonant excitation error of the OR gate from 17% to 0.2%.

In the context of universal fault-tolerant quantum computation, quantum error correction also constitutes a nonunitary process as multiple erroneous processes are mapped to the same corrected state. Our work can be seen as a stepping stone toward an implementation of autonomous quantum error correction, in which erroneous states are coherently mapped to oscillator excitations and are then removed through dissipation [39]. We have demonstrated the required techniques, resonance engineering and sympathetic cooling, in the present experiment [71].

We gratefully acknowledge discussions with Jonathan Home and support by the EU Quantum Technology Flagship grant Advanced quantum computing with trapped ions under Grant Agreement No. 820495 and by the U.S. Army Research Office through Grant No. W911NF-21-1-0007. We also acknowledge funding by the Austrian Science Fund (FWF), through the Special Research Areas BeyondC (FWF Project No. F7109), ERC-2020-STG 948893, and by the IQI GmbH. The research is also based upon work supported by the Office of the Director of National Intelligence (ODNI), Intelligence Advanced Research Projects Activity (IARPA), via the U.S. Army Research Office Grant No. W911NF-16-1-0070. F. R. and E. Z. acknowledge funding from the Swiss National Science Foundation (Ambizione Grant No. PZ00P2_186040) and the Eidgenössische Technische Hochschule Research Grant No. ETH-49 20-2.

E. Z. developed, under the guidance of F. R., the theoretical protocol. M. W. v. M, F. R., P. S., and E. Z. designed the experiment. M. W. v. M. carried out the experiment and analyzed the data. M. W. v. M., P. H., and L. G. contributed to the experimental setup. R. B., T. M., F. R., and P. S. supervised the project. All authors contributed to the manuscript.

[1] International Technology Roadmap for Semiconductors 2.0, Technical report, ITRS, 2015, https://www.semiconductors.org/wp-content/uploads/2018/06/0_2015-ITRS-2.0-Executive-Report-1.pdf.
[2] M. M. Shulaker, G. Hills, N. Patil, H. Wei, H.-Y. Chen, H.-S. P. Wong, and S. Mitra, Nature (London) **501**, 526 (2013).
[3] D. D. D. Ma, C. S. Lee, F. C. K. Au, S. Y. Tong, and S. T. Lee, Science **299**, 1874 (2003).
[4] M. Y. Han, B. Özyilmaz, Y. Zhang, and P. Kim, Phys. Rev. Lett. **98**, 206805 (2007).
[5] S. Sugahara and M. Tanaka, Appl. Phys. Lett. **84**, 2307 (2004).
[6] S. Salahuddin and S. Datta, Nano Lett. **8**, 405 (2008).
[7] F. Chen, H. Kam, D. Markovic, T.-J. K. Liu, V. Stojanovic, and E. Alon, in *Proceedings of the 2008 IEEE/ACM International Conference on Computer-Aided Design* (IEEE, San Jose, CA, 2008), pp. 750–757.
[8] C. Zhou, D. M. Newns, J. A. Misewich, and P. C. Pattnaik, Appl. Phys. Lett. **70**, 598 (1997).
[9] X. Qian, J. Liu, L. Fu, and J. Li, Science **346**, 1344 (2014).
[10] K.-S. Lee and S.-K. Kim, J. Appl. Phys. **104**, 053909 (2008).
[11] P. Andreakou, S. V. Poltavtsev, J. R. Leonard, E. V. Calman, M. Remeika, Y. Y. Kuznetsova, L. V. Butov, J. Wilkes, M. Hanson, and A. C. Gossard, Appl. Phys. Lett. **104**, 091101 (2014).
[12] M. Feng, N. Holonyak, G. Walter, and R. Chan, Appl. Phys. Lett. **87**, 131103 (2005).
[13] J. A. Currivan-Incorvia, S. Siddiqui, S. Dutta, E. R. Evarts, J. Zhang, D. Bono, C. A. Ross, and M. A. Baldo, Nat. Commun. **7**, 10275 (2016).
[14] J. M. Pino, J. M. Dreiling, C. Figgatt, J. P. Gaebler, S. A. Moses, M. S. Allman, C. H. Baldwin, M. Foss-Feig, D. Hayes, K. Mayer, C. Ryan-Anderson, and B. Neyenhuis, Nature (London) **592**, 209 (2021).
[15] F. Kranzl, M. K. Joshi, C. Maier, T. Brydges, J. Franke, R. Blatt, and C. F. Roos, Phys. Rev. A **105**, 052426 (2022).
[16] L. Egan, D. M. Debroy, C. Noel, A. Risinger, D. Zhu, D. Biswas, M. Newman, M. Li, K. R. Brown, M. Cetina, and C. Monroe, Nature (London) **598**, 281 (2021).
[17] L. Postler, S. Heußen, I. Pogorelov, M. Rispler, T. Feldker, M. Meth, C. D. Marciniak, R. Stricker, M. Ringbauer,

R. Blatt, P. Schindler, M. Müller, and T. Monz, Nature (London) **605**, 675 (2022).
[18] J. Herrmann, S. M. Llima, A. Remm, P. Zapletal, N. A. McMahon, C. Scarato, F. Swiadek, C. K. Andersen, C. Hellings, S. Krinner *et al.*, Nat. Commun. **13**, 4144 (2022).
[19] Z. Chen, K. J. Satzinger, J. Atalaya, A. N. Korotkov, A. Dunsworth, D. Sank, C. Quintana, M. McEwen, R. Barends, P. V. Klimov *et al.*, Nature (London) **595**, 383 (2021).
[20] T. Olsacher, L. Postler, P. Schindler, T. Monz, P. Zoller, and L. M. Sieberer, PRX Quantum **1**, 020316 (2020).
[21] C. Zhang, F. Pokorny, W. Li, G. Higgins, A. Pöschl, I. Lesanovsky, and M. Hennrich, Nature (London) **580**, 345 (2020).
[22] S. Krinner, N. Lacroix, A. Remm, A. Di Paolo, E. Genois, C. Leroux, C. Hellings, S. Lazar, F. Swiadek, J. Herrmann *et al.*, Nature (London) **605**, 669 (2022).
[23] P. Hrmo, B. Wilhelm, L. Gerster, M. W. van Mourik, M. Huber, R. Blatt, P. Schindler, T. Monz, and M. Ringbauer, arXiv:2206.04104 (2022).
[24] J. Chu, X. He, Y. Zhou, J. Yuan, L. Zhang, Q. Guo, Y. Hai, Z. Han, C.-K. Hu, W. Huang *et al.*, Nat. Phys. **19**, 126 (2023).
[25] J. Preskill, Quantum **2**, 79 (2018).
[26] K. Bharti, A. Cervera-Lierta, T. H. Kyaw, T. Haug, S. Alperin-Lea, A. Anand, M. Degroote, H. Heimonen, J. S. Kottmann, T. Menke *et al.*, Rev. Mod. Phys. **94**, 015004 (2022).
[27] J. Foldager, A. Pesah, and L. K. Hansen, Sci. Rep. **12**, 3862 (2022).
[28] J. Wu and T. H. Hsieh, Phys. Rev. Lett. **123**, 220502 (2019).
[29] D. Zhu, S. Johri, N. M. Linke, K. A. Landsman, C. Huerta Alderete, N. H. Nguyen, A. Y. Matsuura, T. H. Hsieh, and C. Monroe, Proc. Natl. Acad. Sci. U.S.A. **117**, 25402 (2020).
[30] Y. Wang, G. Li, and X. Wang, Phys. Rev. Appl. **16**, 054035 (2021).
[31] G. Mazzola, P. J. Ollitrault, P. K. Barkoutsos, and I. Tavernelli, Phys. Rev. Lett. **123**, 130501 (2019).
[32] G. Verdon, J. Marks, S. Nanda, S. Leichenauer, and J. Hidary, arXiv:1910.02071.
[33] H. Wang, S. Ashhab, and F. Nori, Phys. Rev. A **83**, 062317 (2011).
[34] L. Del Re, B. Rost, A. F. Kemper, and J. K. Freericks, Phys. Rev. B **102**, 125112 (2020).
[35] Z. Hu, R. Xia, and S. Kais, Sci. Rep. **10**, 3301 (2020).
[36] Z. Hu, K. Head-Marsden, D. A. Mazziotti, P. Narang, and S. Kais, Quantum **6**, 726 (2022).
[37] J. Leppäkangas, N. Vogt, K. R. Fratus, K. Bark, J. A. Vaitkus, P. Stadler, J.-M. Reiner, S. Zanker, and M. Marthaler, arXiv:2210.12138.
[38] I. Cong, S. Choi, and M. D. Lukin, Nat. Phys. **15**, 1273 (2019).
[39] F. Reiter, A. S. Sørensen, P. Zoller, and C. A. Muschik, Nat. Commun. **8**, 1822 (2017).
[40] M. Raghunandan, F. Wolf, C. Ospelkaus, P. O. Schmidt, and H. Weimer, Sci. Adv. **6**, eaaw9268 (2020).
[41] X. Mi, A. A. Michailidis, S. Shabani, K. C. Miao, P. V. Klimov, J. Lloyd, E. Rosenberg, R. Acharya, I. Aleiner, T. I. Andersen *et al.*, Stable quantum-correlated many body states via engineered dissipation, arXiv:2304.13878.
[42] P. M. Harrington, E. J. Mueller, and K. W. Murch, Nat. Rev. Phys. **4**, 660 (2022).
[43] A. Kronwald, F. Marquardt, and A. A. Clerk, New J. Phys. **16**, 063058 (2014).
[44] G. S. Agarwal and S. Huang, Phys. Rev. A **93**, 043844 (2016).
[45] F. Reiter, D. Reeb, and A. S. Sørensen, Phys. Rev. Lett. **117**, 040501 (2016).
[46] M. J. Kastoryano, F. Reiter, and A. S. Sørensen, Phys. Rev. Lett. **106**, 090502 (2011).
[47] Y. Lin, J. P. Gaebler, F. Reiter, T. R. Tan, R. Bowler, A. S. Sørensen, D. Leibfried, and D. J. Wineland, Nature (London) **504**, 415 (2013).
[48] G. Morigi, J. Eschner, C. Cormick, Y. Lin, D. Leibfried, and D. J. Wineland, Phys. Rev. Lett. **115**, 200502 (2015).
[49] D. C. Cole, J. J. Wu, S. D. Erickson, P.-Y. Hou, A. C. Wilson, D. Leibfried, and F. Reiter, New J. Phys. **23**, 073001 (2021).
[50] D. C. Cole, S. D. Erickson, G. Zarantonello, K. P. Horn, P.-Y. Hou, J. J. Wu, D. H. Slichter, F. Reiter, C. P. Koch, and D. Leibfried, Phys. Rev. Lett. **128**, 080502 (2022).
[51] M. Malinowski, C. Zhang, V. Negnevitsky, I. Rojkov, F. Reiter, T.-L. Nguyen, M. Stadler, D. Kienzler, K. K. Mehta, and J. P. Home, Phys. Rev. Lett. **128**, 080503 (2022).
[52] E. Doucet, F. Reiter, L. Ranzani, and A. Kamal, Phys. Rev. Res. **2**, 023370 (2020).
[53] J. T. Barreiro, M. Müller, P. Schindler, D. Nigg, T. Monz, M. Chwalla, M. Hennrich, C. F. Roos, P. Zoller, and R. Blatt, Nature (London) **470**, 486 (2011).
[54] C. Wang and J. M. Gertler, Phys. Rev. Res. **1**, 033198 (2019).
[55] F. Verstraete, M. M. Wolf, and J. Ignacio Cirac, Nat. Phys. **5**, 633 (2009).
[56] E. Zapusek, A. Javadi, and F. Reiter, Quantum Sci. Technol. **8**, 015001 (2023).
[57] M. F. Brandl, M. W. van Mourik, L. Postler, A. Nolf, K. Lakhmanskiy, R. R. Paiva, S. Möller, N. Daniilidis, H. Häffner, V. Kaushal *et al.*, Rev. Sci. Instrum. **87**, 113103 (2016).
[58] See Supplemental Material at http://link.aps.org/supplemental/10.1103/PhysRevLett.132.040602 for Sec. D, where we show that any Markovian evolution on two qubits can be realized by dissipation engineering along with two-qubit unitaries. This section includes Refs. [39,56,59–61].
[59] F. Reiter and A. S. Sørensen, Phys. Rev. A **85**, 032111 (2012).
[60] D. Bacon, A. M. Childs, I. L. Chuang, J. Kempe, D. W. Leung, and X. Zhou, Phys. Rev. A **64**, 062302 (2001).
[61] R. Sweke, I. Sinayskiy, D. Bernard, and F. Petruccione, Phys. Rev. A **91**, 062308 (2015).
[62] The equations describing the dynamics of the system are given in Supplemental Material [58], Sec. A.
[63] J. D. Jost, J. P. Home, J. M. Amini, D. Hanneke, R. Ozeri, C. Langer, J. J. Bollinger, D. Leibfried, and D. J. Wineland, Nature (London) **459**, 683 (2009).
[64] J. P. Home, in *Advances in Atomic, Molecular, and Optical Physics* (Elsevier, New York, 2013), Vol. 62, pp. 231–277.

[65] M. Brownnutt, M. Kumph, P. Rabl, and R. Blatt, Rev. Mod. Phys. **87**, 1419 (2015).
[66] An analytic expression for the error is calculated in Supplemental Material [58], Sec. B.
[67] I. A. Boldin, A. Kraft, and C. Wunderlich, Phys. Rev. Lett. **120**, 023201 (2018).
[68] J. P. Home, D. Hanneke, J. D. Jost, D. Leibfried, and D. J. Wineland, New J. Phys. **13**, 073026 (2011).
[69] M. K. Joshi, A. Fabre, C. Maier, T. Brydges, D. Kiesenhofer, H. Hainzer, R. Blatt, and C. F. Roos, New J. Phys. **22**, 103013 (2020).
[70] G. Morigi, J. Eschner, and C. H. Keitel, Phys. Rev. Lett. **85**, 4458 (2000).
[71] Experimental parameters required to break even in autonomous quantum error correction are provided in Supplemental Material [58], Sec. C.